Title

A stochastic description of pH within nanoscopic water pools

Journal

Cell Reports Physical Science, 4(6)

ISSN

2666-3864

Authors

Li, Sirui

Kwon, Soonho

Goddard, William A

et al.

Publication Date

2023-06-01

DOI

10.1016/j.xcrp.2023.101458

A stochastic description of pH within nanoscopic water pools

Sirui Li,[1,2] Soonho Kwon,[1,3] William A. Goddard, III,[1,3] and Frances A. Houle*[†1,2]

[1]Liquid Sunlight Alliance

[2]Chemical Sciences Division, Lawrence Berkeley National Laboratory, Berkeley, CA 94720, U.S.A.

[3]Materials and Process Simulation Center, California Institute of Technology, Pasadena, CA 91125, U.S.A.

*Correspondence: fahoule@lbl.gov

[†] Lead Contact: fahoule@lbl.gov

SUMMARY

The nature of pH in a pure water pool too small to have a continuous population of ions formed by water dissociation is not settled. We use stochastic kinetics simulations of the water dissociation reaction in pools ranging from 10^3 to 10^{16} waters to characterize water ion lifetimes and populations. An availability coefficient is defined to quantify the intermittent presence of ion pairs during an arbitrary observation period, and used in a proposed definition for the effective pH of nanoscopic pools. The effective pH converges to the bulk value of 7 for water pools in the range of 10^{10} waters. The lifetimes of water ion pairs are found to increase with increasing water pool size due to the balance between their formation and recombination kinetics, with a maximum near the size where bulk-like characteristics begin to dominate and ion pairs are continuously present.

KEYWORDS: Water autoionization, pH, stochastic kinetics, computation, Poisson distribution, lifetime, nanoscopic pool

INTRODUCTION

One of the most important fundamental properties of water is the dynamic equilibrium between H_2O molecules and its ions ($H^{+¿¿}$ and $OH^{-¿¿}$).[1-3]

$$H_2O \rightleftharpoons H^{+¿+OH^{-¿¿}¿} \quad (1)$$

This reaction generates small quantities of water ions that play key roles in many kinds of chemical reactions, the concentrations of which can be controlled by the addition of acids, bases, and salts.[4] The dynamic balance between the activities of $H^{+¿¿}$ and $OH^{-¿¿}$ in aqueous media is quantified as the solution pH, calculated from the equilibrium constant $K_W = 10^{-14}$ for **Eqn (1)**, using the thermodynamic definition

$$K_W = a_{H^{+¿}} \times \frac{a_{OH^{-¿}}}{a_{H_2O}} ¿ \quad (2)$$

where a is activity. Because H_2O is in its standard state, its value for a is defined by thermodynamics to be 1. The thermodynamic definition for pH is given as

$$pH = -\log_{10} ¿ \quad (3)$$

where γ is the activity coefficient for protons at the specified pH, and ¿¿ is the standard proton concentration, defined to be 1 M with an activity coefficient of 1. In solutions where ion concentrations are low, ion pair interactions are assumed to be minimal, and $\gamma = 1$ for $H^{+¿¿}$ and

$OH^{-¿¿}$. This situation applies for water ions in an aqueous solution, particularly near neutral pH, where the ion concentration is many orders of magnitude smaller than the undissociated water concentration. **Eqs (2)** and **(3)** apply to bulk water, however, it has been recognized for some time that as pure water pool volumes become very small, at some point there will be too few waters present to ensure that there will be at least one proton at all times in that pool at a particular pH. [5,6] At pH = 7, when **Eqn (2)** is substituted into **Eqn (3)** the minimum number of waters needed is 10^7. This number corresponds to a spherical pool with a radius of about 42nm. For smaller pools, water ions would be present with an average number of < 1, meaning they can only be present intermittently. This situation is not uncommon in biological systems.[7] For example, techniques have been developed by Shon and Cohen to describe the fluctuations associated with intermittency in terms of Poisson statistics.[8] **Eqns (2)** and **(3)** are no longer strictly valid for these pools, and other ways must be found to describe pH within them. Understanding how chemistry within nanoscopic pools depends on fluctuating concentrations of $H^{+¿¿}$ and $OH^{-¿¿}$ at a quantitative level will advance our understanding of chemistry in systems ranging from cells in living organisms to membrane-electrode assemblies to emulsions, and of acid-base reactions in confined volumes in general.

In the present study, we propose a description of pH in small water pools that is specifically based on the intermittent populations of the water ions in them and is rooted in the thermodynamics and kinetics of water chemistry. We use stochastic chemical kinetics simulations to examine in depth the influence that the chemical equilibrium **Eqn (1)** has on the composition of pure water pools ranging from a few nanometers in size to volumes large enough

to exhibit bulk properties. The modeled system is illustrated in **Figure 1**. The intermittent formation and recombination of OH^- and H_3O^+ has been examined previously for a few dozen waters and very short times (ps) using molecular dynamics techniques,[9,10] providing important information on localized interactions that influence water reactions. Stochastic chemical kinetics using validated rate coefficients allows a much broader exploration of ion pair formation and recombination – spanning many orders of magnitude in time and water pool size – thereby providing key information on how water reactions control the nature of pH from a transient quantity at the nanoscale to its thermodynamically defined characteristics at the bulk scale.

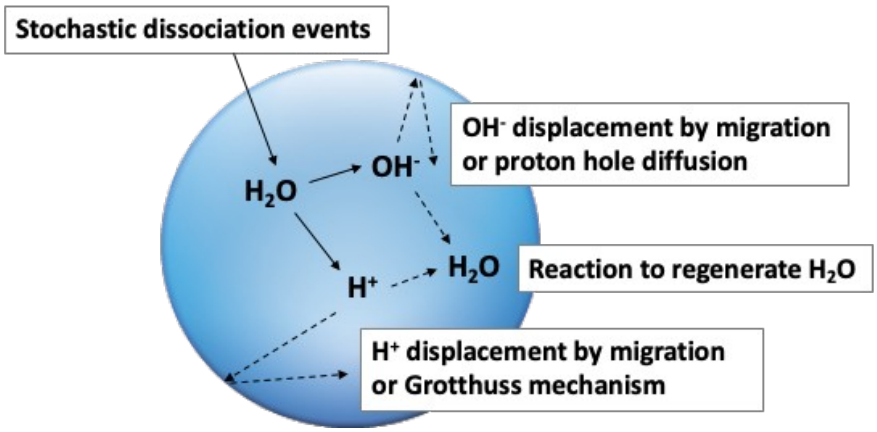

Figure 1. Schematic of the chemistry in a pure water pool. H_2O dissociat.ion events in a water pool generate ion pairs that can separate and later recombine. The simulation volume is assumed to be an instantaneously and uniformly mixed single compartment. Although the diffusion physics are important to describe the dynamics, they are not explicitly included here as discussed in the Computational Methods Section.

RESULTS

Benchmarking the kinetic model against ab initio Molecular Dynamics simulations

We directly compare the predictions of our stochastic kinetics simulations to a previous ab initio molecular dynamics (AIMD) study of water ion recombination by Hassanali *et al.*[10] in a system of 64 H_2O molecules placed in a cubic compartment. This is intended as a benchmark to validate the use of stochastic chemical kinetics at the nanoscale, and to assess any potential impacts of the assumption of a well-mixed volume on the stochastics of water ion pair recombination. In the AIMD study, ion pairs were introduced at the beginning of the calculations to perturb the system away from equilibrium and the recombination process was studied. Their trajectories provided insights into recombination as a function of initial distance between the initial ion pairs, and they generated a statistical distribution for the ion pair lifetimes using them. The resulting lifetime distribution as a function of time after the trajectories were initiated are shown in the upper panel of **Figure 2**. We extracted ion pair lifetimes from the results of stochastic kinetics simulations of a 64-water pool over an observation time *t* of hundreds of seconds using **Eqn (11)** in the Computational Methods Section, and plot them in **Figure 2**, lower panel. Because we simulate both formation and recombination of the ion pairs, we calculate the lifetimes by subtracting the time at which the ion pair is formed from the time at which it recombines.

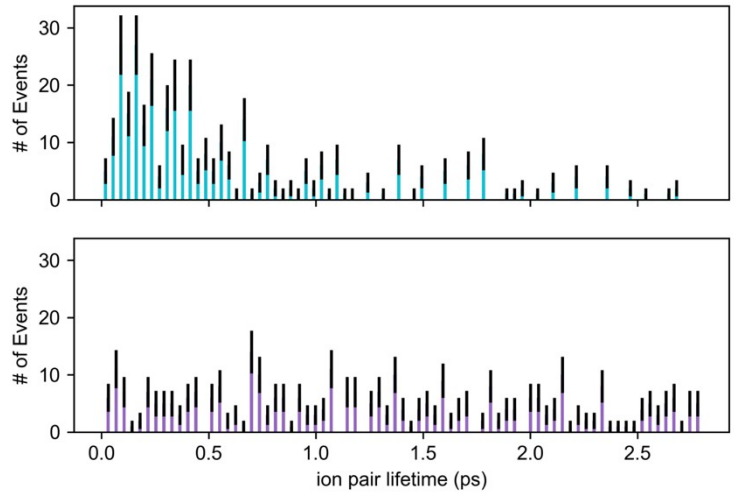

Figure 2. Ion pair lifetime distributions in a pool of 64 H_2O molecules. The upper panel (cyan) is from the AIMD study[10] and the lower panel (purple) is from the stochastic simulations. Both distributions are plotted using 75 bins to span the full time range. The black bars represent the scatter for events obeying Poisson statistics, i.e. $\sqrt{\#\ of\ events}$.

Figure 2 shows that the stochastic simulations do not capture the peak in the statistical distribution found by AIMD for the first 500 fs, attributed to in-cage recombination.[10] Instead, these events are spread out over the entire 2.7 ps time range, and the distribution is flatter. In the prior AIMD study, the influence of the H-bonded water cage on recombination was of particular interest, examining the importance of recombination of ions initially generated within the cage to those generated outside the cage. The overall numbers of ion pairs showing lifetimes up to 2.7 ps is similar in the AIMD and the stochastic kinetics calculations. However, by using a single compartment for the stochastic kinetics, the specific influence of the water cage on ion pair recombination is not accessible. In particular, the physics revealed to be important by AIMD such as a mechanistic step of compressing a H_2O wire structure prior to ion pair recombination is not captured. This compression step was estimated to have a characteristic time of 65 fs. Full 3-D simulations using stochastic kinetics with multiple compartments containing a single water

cage (5-8 waters) can be performed to build in such physical detail however they are highly cumbersome for more than a few compartments when lifetime information is sought, and were not implemented here.

Although information on recombination within the initial water cage is not easily included, because of its computational efficiency the stochastic method can simulate the H_2O reactions for much longer times, providing information on the lifetimes of ion pairs that do not immediately recombine and even on the autoionization reaction of water. The 64 H_2O ion pair lifetime distribution obtained in the stochastic kinetics simulations is a compilation of 21 independent simulation runs examining water ion formation and recombination over a total simulation period of around 500 seconds. Each run was initiated with a different starting random number seed, resulting in distinct sequences of random numbers for event selection and time step calculations. The lifetime data revealed that many pairs have lifetimes of 10s of ps, well beyond the 3 ps time range accessible by AIMD (**Figure 2**). The resulting ion pair lifetime probability distribution normalized to 1 is shown in **Figure 3**.

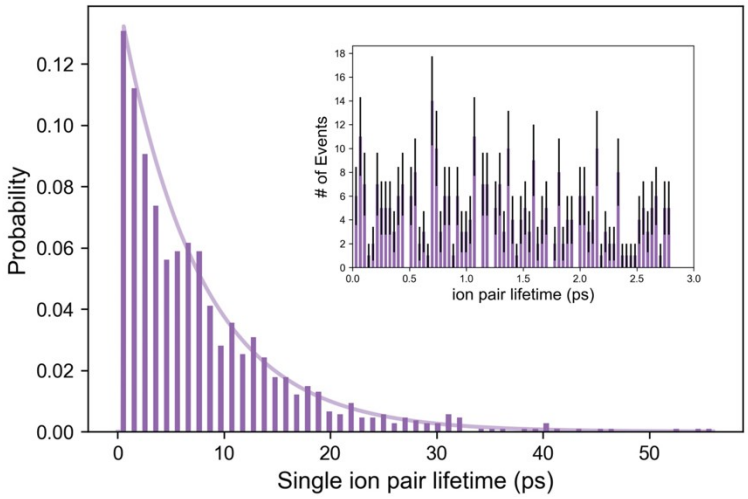

Figure 3. Normalized ion pair lifetime distribution with exponential decay fitting for stochastic kinetics simulations of a 64 H_2O pool. A total of 1050 ion pair lifetime data points are included in the distribution. The figure inset shows 331 ion pair lifetime data points to 2.7 ps (also shown in Figure 2).

Analysis of the 1050 ion pair lifetimes in **Figure 3** using **Eqn (11)** in the Computational Methods Section shows that both the mean ion pair lifetime and its standard deviation have a value of 7.5 ps. According to the stochastic simulations, the shortest observed ion pair lifetime is 12 fs and the longest observed ion pair lifetime is 56 ps. The shortest ion pair lifetime is comparable to the 65 fs lifetime component from the fit to the prior AIMD calculations.

Properties of water pools from 10^3 **–** 10^{10} H_2O

Having examined the consistency between the stochastic kinetics results and AIMD results for a 64-water pool, stochastic simulations of water ion chemistry in the range of water pool sizes that are listed in **Table 1** in the Computational Methods Section and plotted in **Figure 4** were performed to identify key trends. As shown in **Figure 4(B)**, small pools have at most one water ion pair at a time, but as the pool increases beyond 10^6 waters, multiple ion pairs can be present simultaneously.

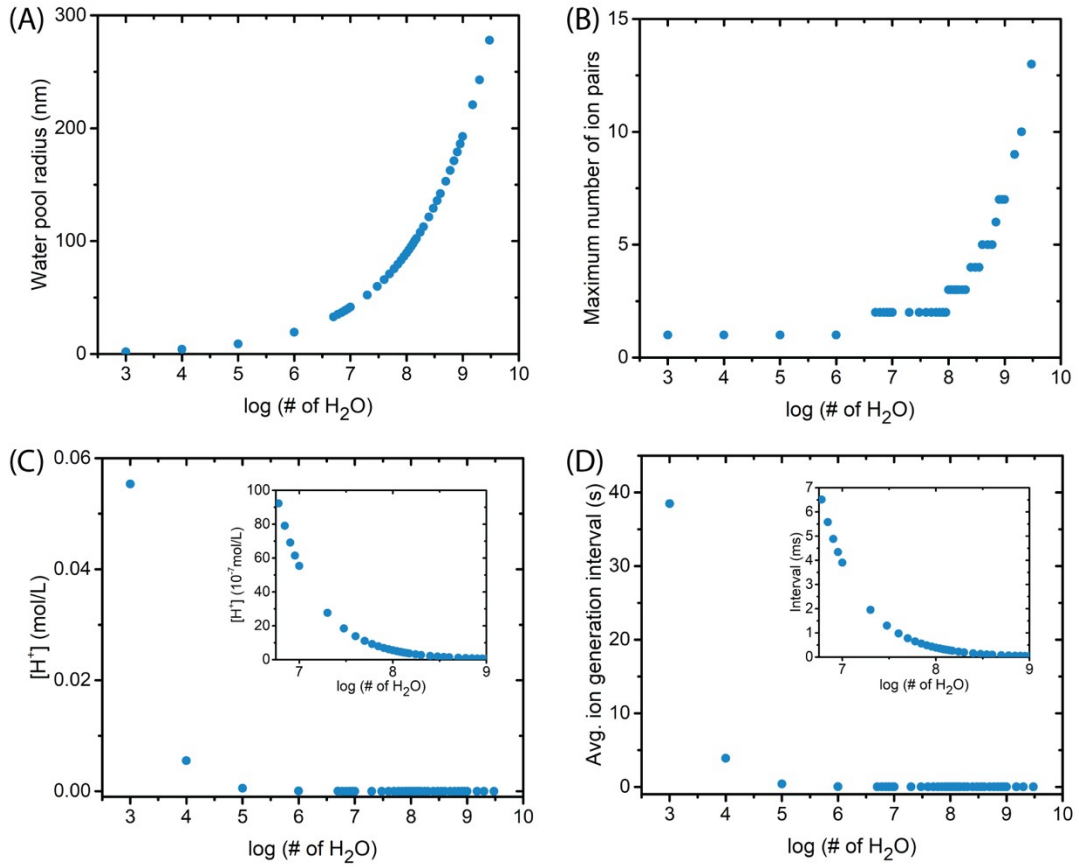

Figure 4. Fundamental properties of H_2O pools as a function of number of waters, ranging from 10^3 to 5×10^9. (A) Pool radius, calculated from the pool volume assuming a spherical geometry; (B) maximum number of ion pairs observed to be present simultaneously; (C)

Average ion pair generation interval; (D) Instantaneous proton concentration for a water pool having a single ion pair only. The insets show details for the water pool range where the intervals and concentrations converge rapidly to bulk water properties.

Trends in water ions relevant to chemical kinetics are shown in **Figure 4**. **Figure 4(C)** indicates that ion pairs are generated much more frequently as the pool size increases, which is expected because there are more chances for water to autoionize in a given time interval when more waters are present. For instance, in pools having 5×10^9 waters the average ion generation interval is 14 μs, while the average wait time between ion generation events is around 40 s for pools having 10^3 waters. The infrequent ion pair formation in extremely small water pools is a result of having only a few H_2O in the tail portion of the thermal Boltzmann distribution with sufficient internal energy to undergo autoionization.[11] **Figure 4(D)** shows concentration trends with pool size. When a single ion pair is present in pool having fewer than 10^8 waters, the corresponding instantaneous ¿¿ or ¿¿ is much higher than 10^{-7}M, the value expected for bulk pure water in its standard state at chemical equilibrium. This is entirely due to the small volumes of the pools. Shon and Cohen have also pointed out that reactant concentrations subject to small volume confinement are high.[8] Higher concentrations of reactants lead to faster reaction kinetics. In this study, the higher water ion concentrations in the smaller pools lead to shortened ion lifetimes within them.

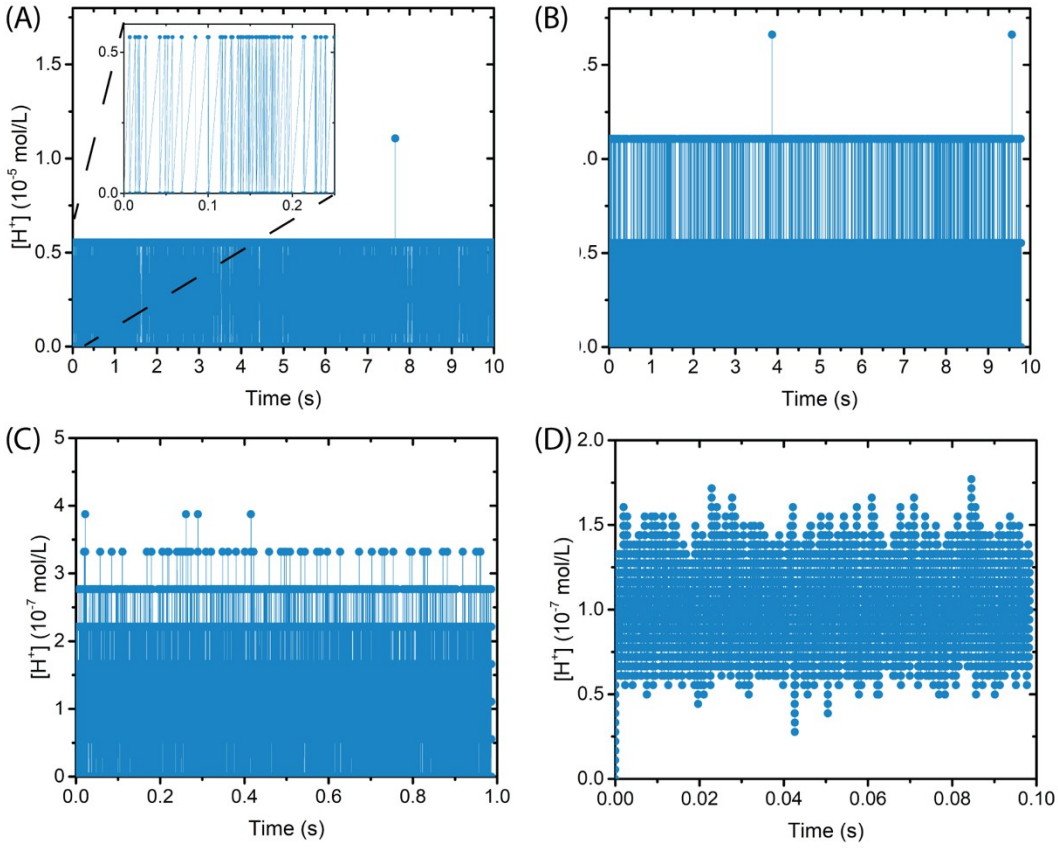

Figure 5. $H^{+¿¿}$**concentration profiles as a function of water pool size, simulated for specific time periods.** (A) 10^7 H_2O, 10s, with inset showing details to 0.25 s; (B) 10^8 H_2O, 10s; (C) 10^9 H_2O, 1s; (D) 10^{10} H_2O, 0.1s.

Details of proton concentration stochastics as a function of water pool size are shown in **Figure 5**, for pools containing 10^7, 10^8, 10^9 and 10^{10} H_2O molecules. The data show every formation and recombination event occurring during the simulation period: each spike in proton concentration corresponds to an ion pair generation event, and each dip in proton concentration correspond to an ion pair recombination event. The four panels reveal the transition from single ion pairs being present sporadically to multiple ion pairs being present continuously. For the case of a pool containing 10^7 H_2O (**Figure 5(A)**), having more than one ion pair present at a time is a

rare event. The pool contained two ion pairs on only one occasion for this simulation run. As the water pool sizes increase, instances when multiple ion pairs are present become more frequent. As shown in **Figure 5(D)** for a 10^{10} H_2O pool, generation of ion pairs outpaces recombination from the very beginning until a steady state condition is reached, where ion pairs are always present. At steady state, the ion concentrations are on average ¿¿mol/L. The data in **Figure 5** indicate that a water pool of 10^{10} waters can sustain a consistent presence of ion pairs (albeit with a fluctuating population of ion pairs), whereas smaller pools cannot.

Ion pair lifetimes and mean diffusion distances

The simulation data tracking individual ion pair formation and recombination events allow the lifetime of a transient ion pair to be extracted. Because the particles represent molecules, water ions are indistinguishable in the simulations. Only lifetimes calculated from observation times where just one pair is present can uniquely be assigned to the process of forming and recombining that particular pair, so only those data are used for lifetime estimates. We use **Eqns (5)** and **(6)** and the single ion pair lifetime distributions shown in **Supplemental Information Note S1 Figure S1** and **Note S2 Table S1)** to determine mean ion pair lifetimes as a function of water pool size. The results are shown in **Figure 6(A)** (cyan).

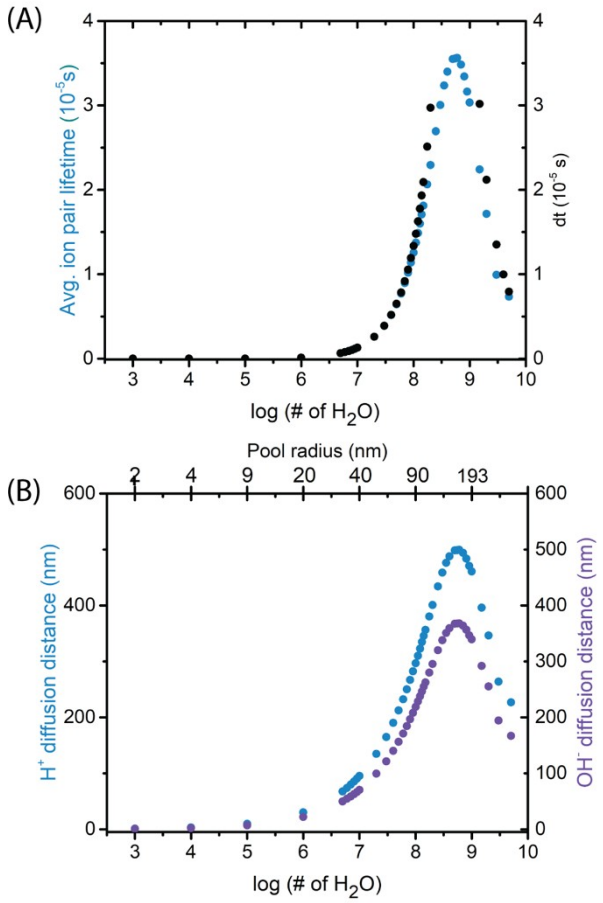

Figure 6. Ion pair characteristics as a function of water pool size. (A) Ion pair lifetimes. The data in cyan are from the simulations, corresponding to when only one pair is present. The data in black are lifetimes for a single pair calculated from the rate equations (4) and (5) as a function of water pool size. Data points approaching the singularity as the denominator in Eqn (8) approaches zero are omitted from the plot but are provided in Table S1. (B) Water ion diffusion. Estimated diffusion distances for $H^{+¿¿}$ (cyan) and $OH^{-¿¿}$ (purple) ions based on the self-diffusion coefficients are shown with the corresponding mean ion pair lifetime data. The upper x-axis shows the pool radii from Table 1 in the Computational Methods Section for the corresponding pool size (lower x-axis). See also Figures S1 and S2.

Figure 6(A) shows that the single ion pair lifetime extracted from the simulations initially increases as pool size increases, reaching a maximum lifetime at around 5×10^8 H_2O. Further increases in pool size lead to a decrease in the calculated ion pair lifetime. To

quantitatively explain this behavior, we consider the deterministic rate expression for disappearance of a single H^{+}¿¿ in a specific pool size, derived from **Eqn (1)**

$$-d¿¿¿ \tag{4}$$

The left-hand side of **Eqn (4)** is the rate of disappearance of a H^+ in a time interval *dt*, where the specific condition of conversion of a pool having one H^+ to a pool having no H^+ is indicated by the subscript $1 \rightarrow 0$. On the right-hand side of **Eqn (4)**, $k_D[H_2O]$ is the ion pair generation rate for the pool and k_R¿¿ is the instantaneous ion pair recombination rate when there is only one ion pair present in the pool (i =1). The recombination rate is represented as being second order in $[H^+]$ for mathematical convenience because ¿¿ is always equal to ¿¿ in pure water. The generation rate is essentially constant for all water pool sizes because the dissociation of one water has minimal impact on $[H_2O]$. The recombination rate for a single ion pair, however, decreases nonmonotonically with increasing pool size because the ion concentrations decrease, as shown in **Figure 4(D)**. As described in **SI Note S2**, we rearrange **Eqn (4)** to calculate *dt* from the rate equation,

$$dt = d¿¿¿ \tag{5}$$

where *dt* is now an estimate of the ion pair lifetime for a specific water pool size. Calculations of *dt* for each water pool size are presented in **Figure 6(A)** (black).

Figure 6(A) shows that there is good agreement between the lifetimes estimated using **Eqn (5)** and **Eqn (11)** in the Computational Methods Section, and that the maximum value of *dt* with pool size corresponds to the maximum of mean ion pair lifetime. As shown in **SI Table S1**,

the deterministic rate expression **Eqn (5)** almost perfectly predicts the ion pair lifetime for pool size containing less than 10^8 waters. Beyond this size, however, **Eqn (5)** overpredicts the ion pair lifetime by a value that reaches an order of magnitude at the peak, corresponding to a water pool size of $5 \times 10^8 \, H_2O$. We attribute the deviation to the fact that the denominator of **Eqn (5)** approaches zero as the instantaneous rate of recombination approaches that of generation, and dt becomes undefined. As the H_2O pool size increases further, the presence of multiple ion pairs becomes more prevalent **(Figure 4(B))**. When there are multiple ion pairs, the mean ion pair lifetime decreases. This is because the rate of ion pair recombination increases while the rate of their generation remains essentially constant (**Eqn (4)**). As a result, the mean lifetime presented in **Figure 6(A)** (cyan), which is calculated when only one ion is present in the pool, should be considered to be an upper bound to the true lifetimes of ion pairs in larger pools. **SI Note S3 Figure S2** shows how the presence of multiple ion pairs affects the mean ion pair lifetimes estimated using **Eqn (5)**.

Taking the mean ion pair lifetimes in **Figure 6(A)**, we can estimate the diffusion distance for separated proton and hydroxide ions during their lifetime within a pool using

$$distance = \sqrt{D_{ion} dt} \tag{6}$$

where D_{ion} is the self-diffusion coefficient for the ion. Agmon has estimated that $D_{H^+} = 7 \times 10^{-5} cm^2/s$ by subtracting the H_2O self-diffusion coefficient, $2.3 \times 10^{-5} \, cm^2/s$, from the proton diffusion coefficient, $9.3 \times 10^{-5} cm^2/s$.[12] We estimate the hydroxide self-diffusion coefficient D_{OH^-} using the conductivity measurements reported for protons ($C_{H^+} = 3.62 \times 10^{-3} cm^2 V^{-1} s^{-1}$) and hydroxides

$C_{OH^-}=1.98\times10^{-3}\,cm^2V^{-1}s^{-1}$,[13] and assuming that $D_{OH^-}=D_{H^+}\times\frac{C_{OH^-}}{C_{H^+}}$ = 3.8 x 10^{-5} cm^2/s. Using the values for mean ion pair lifetimes compiled in **SI Table S1**, the ion pair diffusion distance as a function of H_2O pool size is as shown in **Figure 6(B)**.

Figure 6(B) indicates that both proton and hydroxide can undergo significant displacements before recombining. For a pool of 5×10^8 H_2O, which has the longest single ion pair lifetime (3.55 x 10^{-5} s), the estimated diffusion distance is on the order of 500 nm for protons and 300 nm for hydroxides, respectively. The distances are comparable to or larger than the water pool sizes (**Table 1** in the Computational Methods Section), indicating that the ions are likely to be found anywhere in the pool if they do not immediately recombine within their water cage after formation, supporting the assumption made in the Computational Methods Section that the water pools can be considered to be well-mixed. This prediction by the stochastic kinetics simulations is consistent with the study by Geissler et al[9] of the role of molecular-level fluctuations in the recombination process, pointing out that changes in local water structure could result in large separations between ion pairs. In the present work, the rate coefficients for recombination and diffusion capture these physics.

Ion availability coefficient $\alpha_{i>0}$

To quantify the intermittency of ion pairs in a small pool and understand how the intermittency evolves as a function of water pool size, we use the simulation results to determine the timespans during which one ion pair τ_1, two ion pairs τ_2, three ion pairs $\tau_3$etc, are present in a pool of a specific size. These times τ_i can be summed to calculate the total time during which *at*

least one ion pair is present in that pool (i.e. τ_i for i >0) during an observation time. We then normalize this sum by the observation (simulation) time $T_{¿}$ (equal to t in the general Poisson distribution, **Eqn (10)** in the Computational Methods Section) to calculate a dimensionless availability coefficient, $\alpha_{i>0}$ for that pool size. This coefficient represents the intermittent presence of ion pairs in the nanoscopic pool:

$$\alpha_{i>0} = \frac{\sum_{i=1}^{n} \tau_i}{T_{¿}} \tag{7}$$

where n is the maximum number of ion pairs observed to be formed simultaneously in a pool of a given size (**Figure 4(B)**). For small pools that cannot sustain more than one pair of ions (i.e. i = 1), $\tau_{i=1}$ is then equal to dt in **Eqn (5). Figure 7** shows $\alpha_{i>0}$ for pool sizes between 10^3 to 10^{10} waters at two temperatures (25℃ and 37℃). The trend with temperature shows that the pool size for which pH is not defined is temperature-dependent. This dependence primarily reflects a shift of the equilibrium constant $K_{W'}$ in **Eqn (9)** in the Computational Methods Section toward a more frequent generation of ion pairs as temperature increases. **SI Note S4** lists the values plotted in **Figure 7** and T_{sim} for each case.

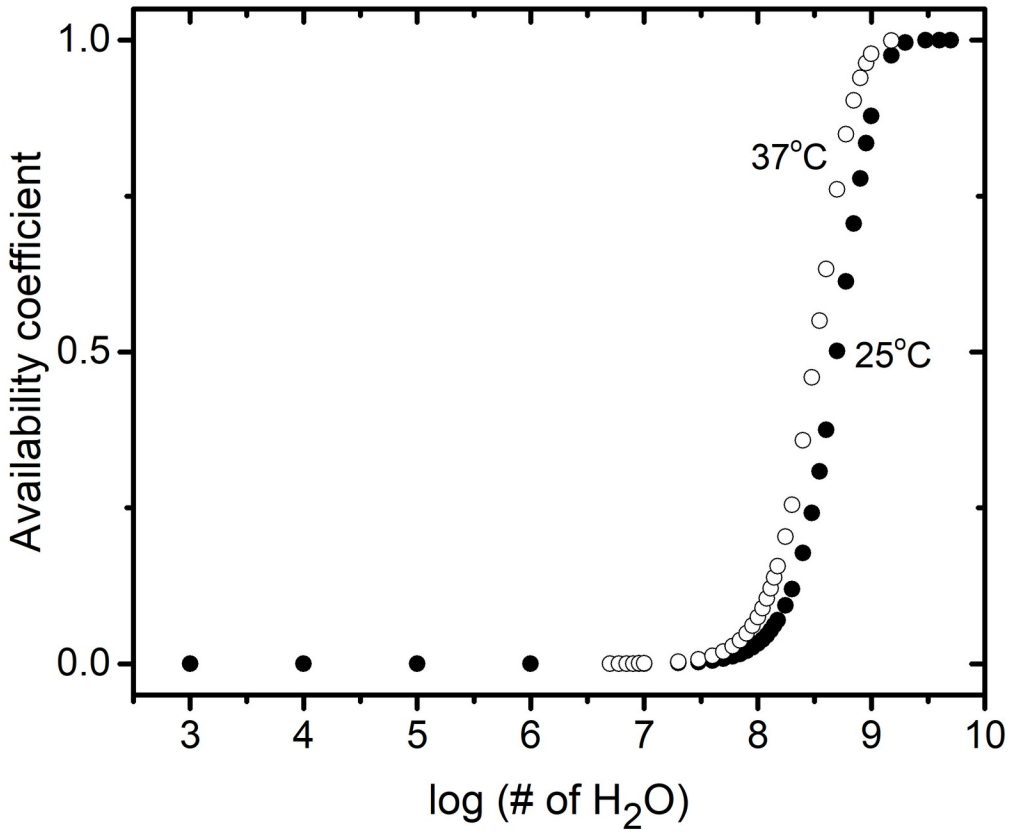

Figure 7. Availability coefficient, $\alpha_{i>0}$,as a function of water pool size at two temperatures. The temperatures 25℃ and 37℃. are selected to evaluate the value of $\alpha_{i>0}$ in typical situations where small water pools may be involved: ambient room temperature and physiological temperature. See also Table S2 and Figure S3.

Figure 7 shows that there is a transition of $\alpha_{i>0}$ from a very small value to unity as water pool sizes increase, which corresponds to a transition from ion pairs being present in a pool intermittently to being present continuously (**Figure 5(D)).** To visualize this transition, we show the contributions of specific numbers of ion pairs (**Figure 4(B)**) to $\alpha_{i>0}$ for a pool of 10^7, 5×10^8, 10^9 and 2×10^9 H_2O in **Figure 8**. In the case of 10^7 waters, where the maximum number of ion pairs observed to be present at a time is two (**Fig. 4(B)**), for 99.967% of the observation

time no ion pairs are present in the pool. As the pool size increases, the period of time during which no ions are present decreases, and eventually a persistent population distribution of ion pairs develops. The complementary value $1-\alpha_{i>0}$ gives the probability for H_2O to exist in its undissociated form, (**SI Note S5 Figure S3**).

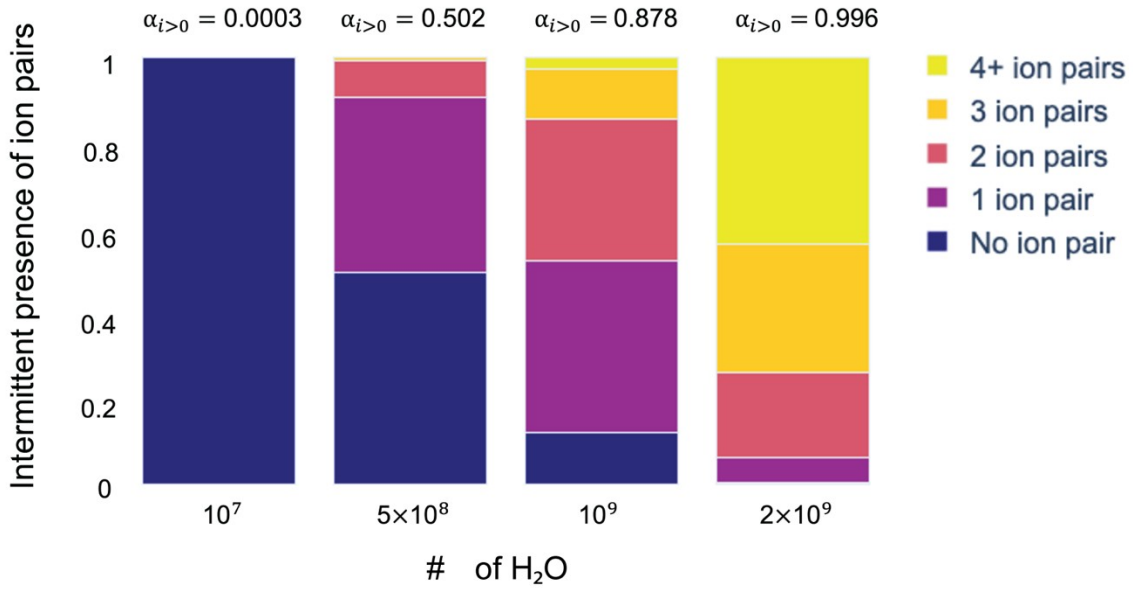

Figure 8. **Fraction of time ion pairs are present in selected water pools.** This is shown using a breakdown of the availability coefficient $\alpha_{i>0}$ into contributions from the number of ion pairs present during the observation time.

Effective pH in small water pools

Based on the simulation data, we propose a quantitative expression for the effective pH in small water pools, where there is no pH for periods of time, as an extension of **Eqn (3)**. The phrase effective pH has two common meanings in the literature: the pH range over which a buffer system with a particular pKa can maintain a desired pH (or buffer capacity[14]), and the apparent pH for systems where direct measurement of pH is challenging.[15] We use the term in

this second sense, with a specific focus on defining what effective pH is at the nanoscale. We start from the thermodynamic concept of an activity coefficient ɣ, which measures the fraction between zero and one of a chemical species that is available to react in ideal and non-ideal solutions. ɣ is taken to be 1 for species in dilute solutions where interactions beyond simple solvation are minimal, meaning that the species can always react. The availability coefficient $\alpha_{i>0}$ for H^+ is << 1 for pools in the range of 10^7 waters or less (**Figure 8**). This means that protons are mostly not present, so cannot react, and we propose that this means that ɣ should also be << 1. By equating $\alpha_{i>0}$ with ɣ, we introduce a way to measure protons being present in the pool for very short periods of time and being completely absent the rest of the time, extending **Eqn (3)** to the transient regime. The other key term in **Eqn (3)** is $[H^+]$, the concentration of protons when they are present, which is pool-size-dependent and much larger than 10^{-7} mole/L in pools of 10^7 waters or less (**Figure 4(D)**). For example, a pool of 10^7 waters would have a pH of about 5 for 1 μs every 5 ms or so (**Figure 4(C)**), and no pH the rest of the time. Combining the availability coefficient and the instantaneous concentration results from the simulations, and taking $[H+]_0$ to be 1 in its standard state, we obtain **Eqn (8)**

$$effective\ pH_{(¿\ of\ H_2O)} = -\log ¿ \tag{8}$$

where α_i is the availability coefficient for a specific water pool size as defined in **Eqn 7**, and ¿¿ denotes the instantaneous molar concentration of protons when *i* pairs are present in that pool. The trend in effective pH with water pool size is shown in **Figure 9**.

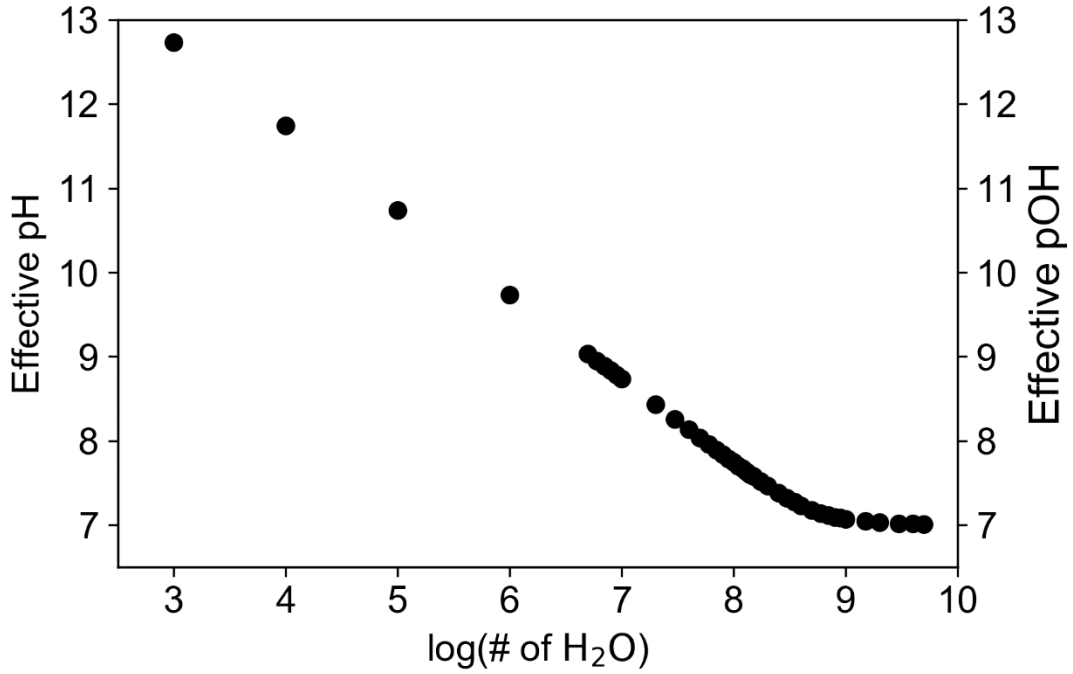

Figure 9. Effective pH and pOH as a function of water pool size. In pure water pools too small to be bulk-like, with a persistent population of protons and hydroxides, K_w no longer applies and the effective pH is equal to the effective pOH.

In the smallest volume (10^3 H_2O), the effective pH = 12.7, decreasing to 7 as the water pool size increases. **Eqn (8)** can also be used to calculate the effective pOH because ¿¿ for pure water. Because thermodynamic equilibrium is not defined in this pool size range, pH and pOH do not add up to 14 as they would in the bulk. **Figure 4(C)** and **Figure 9** together suggest that due to the long periods of time during which no water ions are present in water pools smaller than 10^9 waters, the influence of the reactive environment in the pool on redox chemistry is not the one we understand based on bulk water properties. Chemical reactions that are sensitive to acid will be in a microenvironment where acid is absent much of the time, and is therefore functionally alkaline. An analogous situation applies to chemical reactions sensitive to base.

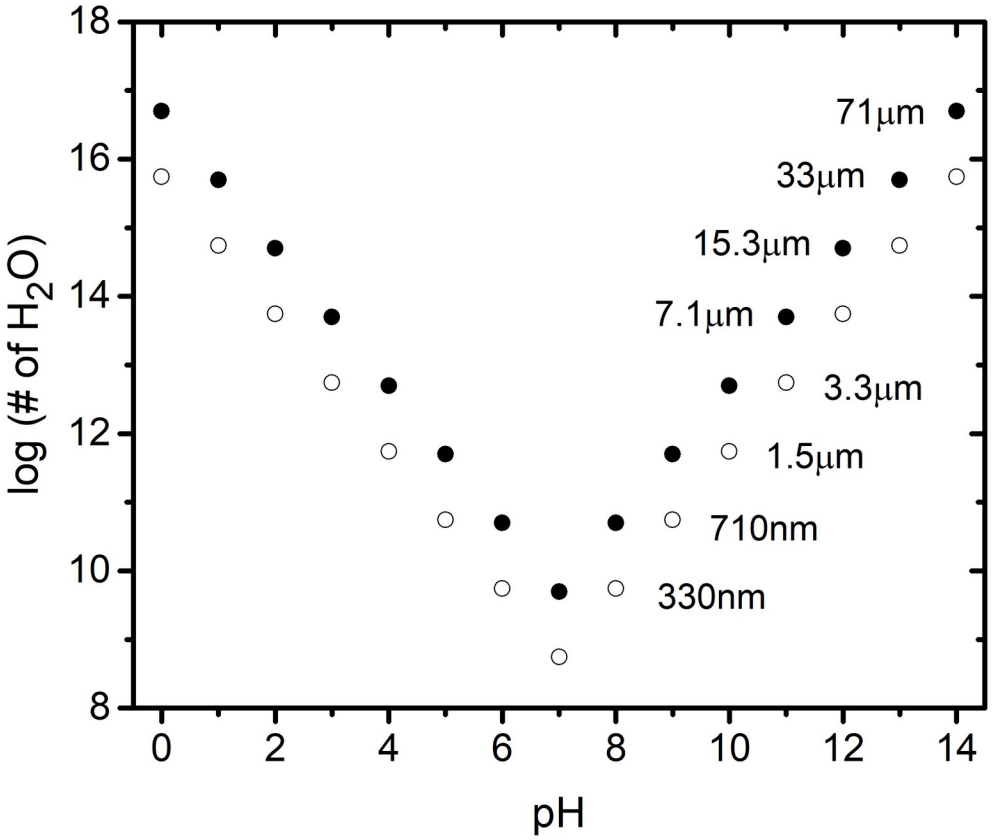

Figure 10. Minimum number of H_2O required to have a thermodynamically defined pH. Two sets of criteria are compared. The open circles are calculated assuming that there must be at least one molecule of both H_3O^+ and OH^- present in the pool on average for pH to be defined, as described by Bal et al (Ref [5]). The closed circles, calculated in this work, satisfy the requirements that the effective pH has converged to a stable value and that at least one of each ion is present nearly 100% of the time for the pH of a pool to be defined. The associated pool radii for the points are shown.

The analysis shown in **Eqn (8)** and **Figure 9** can be used to estimate the minimum pool size required to have a bulk-like pH at pHs other than neutrality, shown in **Figure 10**. We have carried out additional stochastic simulations for acidic solutions by adding excess protons corresponding to the desired pH from pH = 0 to 6. OH^- is present intermittently in these pools when they are too small to have bulk-like properties. We use two criteria to determine when pools are bulk-like: OH^- must be present at all times in the pool (availability coefficient for OH^-

very close to 1), and the pool's effective pH must have converged to a constant value. This ensures that the pool is at thermodynamic equilibrium, that is, K_w is valid and pH + pOH = 14. We find that 8-9 water ion pairs must be present in a pool on average for both criteria to be satisfied at pH 0 to 6. Below this size limit, the fraction of time during which there are no ions and pH is undefined becomes significant. By symmetry these results also apply to alkaline environments, and the acidic results are mirrored to generate minimum pool sizes for pH 8 - pH 14. Our results are compared in **Figure 10** to a similar analysis by Bal et al,[5] which used the criterion that on average at least one H_3O^+ and at least one OH^- must be present in a pool, a more relaxed requirement than continuous presence. The predicted minimum pool sizes for bulk-like properties are significantly smaller.

DISCUSSION

Water can be confined within a nanoscopic volume in natural and artificial microenvironments involving porous and roughened materials as well as biochemical organelles. These microenvironments are often complex, which makes describing and controlling the water content and directly probing water ion chemistry in them challenging, especially when the volumes are likely to be too small to have bulk-like properties. The lack of a clear definition of pH within them has led by necessity to a blurring of bulk, thermodynamically defined pH with concepts of local acidity and basicity, for example in reverse micelles,[16] membrane-electrode assemblies,[17] at electrodes[18] and in aerosol.[19] This blurring points to an opportunity to improve our understanding of chemistry in confined nanoscale volumes through development of a systematic and quantitative description of how protons influence chemistry within them. The stochastic simulations presented here are a first step toward such a definition. We show that

water ions are best described as being sporadically present in these types of nanoscopic pools. When they are present, their instantaneous concentration is much higher than they would be in bulk water, $[H^{+¿¿}] = 10^{-7}$mol/L at 25℃ (**Figure 4(D)**). When they are absent, which is most of the time until the pools reach a diameter in the range of 200 nm (**Table 1** in the Computational Methods section and **Figure 8)**, there is no pH. Accordingly, acidity and basicity within these pools should be seen as a time-averaged combination of transient pH when ions are present, defined as in **Eqn (3)**, and pure water with no ions. The simulations allow this combination to be quantified, resulting in an overall effective pH that characterizes the average aqueous microenvironment.

The existing literature clearly anticipates the sporadic nature of the presence of water ions in pools too small for K_w to apply. Goch and Bal[20] point out that the stochastic nature of generic chemical reactions dominates at the picoliter volume and leads to an apparent equilibrium constant that can deviate significantly from the bulk value. The effective pH defined in **Eqn (8)** and plotted in **Figure 9** conforms to the thermodynamic definition for pH (and the analogous expression for pOH), however because the effective pH + pOH > 14 the apparent equilibrium constant for small pools is expected to be very different from the bulk value. The criterion that both water ions must always be present in the pool for the pool to have bulk-like properties provides a simple way to determine assess whether the chemical kinetics in a pool of a given size are likely to be governed by intermittency or by bulk properties.

We provide a size estimate in **Figure 10** for when a water pool can be considered to have bulk-like properties according to thermodynamics. This estimate is systematically larger than that reported by Bal *et al.*[5] because of the requirement that both water ions be present continuously rather than on average. Which of these criteria is best, or whether other criteria should be used is worthy of study: it is not immediately clear whether in practice one is more accurate than the other for characterizing the properties of reacting chemical systems. Both show the same key trend, however, that the minimum pool size for bulk-like pH to be present increases rapidly with pH. Bal *et al.*[5] discuss this trend in terms of the sizes of biological structures and how to understand their reported internal pH values, which are generally at near-neutral pH. The central question of whether a nanoscopic volume has bulk-like properties also applies to inorganic systems. Cathodes and anodes for (photo)electrochemical fuel generation can involve aqueous environments that are much more acidic or basic than biological ones, and these environments can change during operation.[21,22] When these electrodes are nanostructured, the size of the resulting pools and their degree of connectivity with the bulk electrolyte can result in much larger, semi-isolated volumes whose pH is not defined. As an example, during electrochemical CO_2 reduction the measured pH of the electrolyte near the cathode can increase from 6.8 to around 11.[23-25] Assuming that the structural influence of interfaces on water ions can be neglected, the minimum spherical pool diameter for pH to be thermodynamically defined at all times near the electrode would then increase from about 600nm to about 14 μm during this reaction.

436 Reactions that depend on the availability of protons, such as the hydrogen evolution
437 reaction in acid, or hydroxide ions, such as metal cation hydrolysis in base, obtain them via
438 interfacial dissociation of intact H_2O most of the time. If such direct water dissociation is not
439 feasible, acid- or base-dependent reactions in reacting systems can only occur following the
440 infrequent generation of ion pairs, albeit with a much longer waiting period in between events. In
441 such a situation the dynamics of where the ion pair is formed relative to the reaction center, how
442 big the pool is (governing instantaneous concentrations) and how far the ions can travel before
443 they recombine become important.
444
445 What do experimental results tell us about whether pH in a small pool looks bulk-like or
446 not? Direct measurements on pure water pools without encapsulating molecules in the submicron
447 size range (for example, in aerosol form) have not been reported, although the pH of aqueous
448 aerosol containing salts in the 1-20 μm range has been investigated by Raman spectroscopy.[19,26]
449 There is, however, a rich literature on the structure of water in contact with hydrophobic walls.
450 Some examples include pure water droplets in hydrophobic fluids,[27] and reverse micelles (RM),
451 which are nanoscopic water pools surrounded by non-ionic, anionic or cationic surfactant
452 molecules in an organic solution.[28,29] The size of RMs is characterized using the value W_0, which
453 is the molar ratio of water to surfactant concentration in the RM solution. RMs typically range in
454 size from W_0 = 0 to 70 for many systems,[30] and a water pool with W_0 = 40 contains about 3 x 10^5
455 waters,[6] corresponding to a pool whose volume would have a radius of about 13 nm if spherical.
456 For all surfactants, water in RM is in two distinct interior regions, that next to the surfactants and
457 that toward the center of the enclosed water pool.[6] These regions have been studied using probe
458 molecules to reveal their structure and evaluate pH within them. Optical spectra of probes such

459 as phosphate,[31] sucrose,[32] and vanadate [16] introduced into RM and biological organelles have
460 been used to evaluate pH in these small pools. Water pools with $W_0 > 20$ have properties
461 consistent with the presence of free water at their centers.[33] Proton nuclear magnetic resonance
462 showed that the surfactant dominates the measured pH for $W_0 = 15$ or less.[34] The spectroscopy
463 studies have identified pH gradients within the RM, with pH next to the walls being lower
464 (higher proton concentration) than in the middle.[16] That a gradient could be present is supported
465 by a Poisson Boltzmann model to described the charge distribution within RM resulting from the
466 presence of surfactants and counterions to form the micelle walls.[15]
467
468 RM pool sizes are clearly too small to have a pH most of the time as noted by Bal[5] and
469 quantified in the present study. Proton-hydroxide pairs are formed from time to time, however,
470 and can react with probes before they recombine. Therefore these probes report on their chemical
471 states in confinement compared to bulk solutions, not necessarily on free proton or hydroxide
472 concentrations.[5,35] The structural inhomogeneity of water within the RM[36] complicates
473 interpretation of the spectra: the use of probe spectra has been suggested to only provide an
474 *apparent* pH.[31] It has been recognized that using bulk pH concepts and calibration data to
475 interpret the spectroscopy experiments is not ideal but necessary because of the lack of
476 alternative ways of quantifying the activity of $H^{+¿¿}$ in the complex RM environment.[6]
477
478 It is evident that the chemical relationships resulting from water dissociation into its ions
479 in RM and in bulk liquid remain to be fully characterized. New work addressing this question
480 would be immensely valuable for our understanding of water pools in RM and in other types of

matrices such as nanoporous materials and organelles. Using suitable probes, it is possible that techniques such as single molecule localization microscopy could provide information on proton stochastics in addition to their use as diffusion monitors.[37] Stochastic kinetics simulations extending the present work can be used to interpret such measurements, and to develop a physical picture of the protons within such environments, which are central and ubiquitous in technologies and in nature.

A significant result of the present study is that the lifetime for a single ion pair in pure water varies from 12 fs (i.e. shortest lifetime calculated for 64 H_2O) to 394 μs (i.e. longest lifetime calculated for 5.56×10^8 H_2O), as determined using fits to the Poisson distributions (**Figure 6(A)**). Both ions can have significant diffusion distances within these times relative to the size of the volumes containing them, assuming that the diffusion coefficient is in the same range as in bulk water. Under this assumption, for example, a separated ion pair generated inside a RM with a diameter of 2-40 nm,[38] has a sufficient lifetime (on the order of 10^{-10} to 10^{-7}s) for H+ to diffuse from about 1 to 30 nm and for OH- to diffuse from 0.7 to 22 nm prior to recombination. This lifetime range implies that water ion distributions in the interior of RM would be well-mixed, recognizing that the regions immediately adjacent to the surfactant walls have a separate character that may influence their dynamics. The simulation framework and analysis can be readily adapted to include the influence of organic or inorganic walls surrounding the water volumes, and incorporate solutes to estimate their impact on the size dependence for when pools acquire bulk-like properties. Whether walls and solutes are present or not, no spatial inhomogeneities are likely to be continuously present in the interior of nm-scale pools.

COMPUTATIONAL METHODS

Resource Availability

Lead Contact

The lead contact is Frances A. Houle

(fahoule@lbl.gov)

Materials availability

This computational study did not generate any materials.

Data and Code Availability

The data used to prepare the Figures in this work are available from Zenodo: 10.5281/zenodo.7806995. Standard Python library functions were used in scripts for the Poisson statistics calculations, no new software was written.

Methods Overview

In this study, we investigate a single reversible reaction**, Eqn (1)**, taking place in water pools of varying size (**Figure 1**). The size range spans pools large enough to have bulk-like properties down to nanoscale pools containing 10^3 waters. As noted in the Introduction, a pool must have a minimum size to have persistent water ions, below that size the ion pairs are only present from time to time. This fluctuation in ion pair concentrations within the pools cannot be modeled using continuum, deterministic methods as has been pointed out in early publications.[39,40] As discussed

below, stochastic methods have been developed to simulate chemical kinetics in such systems that treat the reaction steps as a collection of probabilities, unlike deterministic methods that determine a smooth function that can describe the system at all points in time. We describe the stochastic method used for this work, then present the mechanistic elements used in the simulations, and the Poisson statistical analysis used to analyze the simulation results.

Stochastic chemical kinetics method

The computational method used in this work is stochastic chemical kinetics,[39,41,42] which provides a rigorous solution to the master, or time evolution, equation for the species in the system according to the steps in their reaction mechanism.[42] Stochastic chemical kinetics calculations for very simple reversible reactions like **Eqn (1)** can be made using analytical methods to solve for concentrations in reacting systems,[40,43] however the analytical expressions are not readily derived for systems where the average concentration of certain components is less than one molecule in the entire volume, or where strong fluctuations in concentrations occur.[39] As an alternative, stochastic chemical kinetics calculations using an iterative algorithm involving random selection of probability-weighted events as described by Bunker and later Gillespie provide an accurate solution for a broader set of cases.[41,42] The advantages of this algorithm are that it is accurate and suitable for predictive simulations of a wide range of complex chemical systems.

We use an open-access implementation of the Bunker-Gillespie stochastic chemical kinetics method, the Kinetiscope code package.[44] In this simulator, populations of reactants and products are represented using particles, where each particle is defined to be a certain number of

molecules. For the present simulations, each particle is set to represent a single molecule so that the detailed statistics could be captured. To perform the simulations, the reaction steps (Eq (1) in this case), the associated rate coefficients, and the dimensions of the water pool are the only inputs required. The reaction steps and their associated rate coefficients fully describe the conversion of reactants to products. They and the reactant populations present are used to calculate instantaneous reaction rates, which are equated to reaction probabilities by normalizing them to the total of all rates at each point in time. The next reaction event is randomly selected among the probability-weighted mechanistic steps, the populations of species updated using the stoichiometry of the selected step, and the associated time step is calculated from the total of all rates. If the rate coefficients and populations are accurate, the time step is accurate and the overall time base for the calculation is absolute. After this sequence, probabilities are recalculated and a new event selection cycle begins. In order to capture the full statistics, the state of the system is saved after every event in the present study. The dynamic range of time intervals between events accessible by this method is limited by the 64-bit accuracy of the computer's microprocessor. In this study we have resolved ion lifetimes of femtoseconds (fs) with ion formation events spaced by many seconds.

Stochastic Model Construction

We model the forward reaction as a unimolecular dissociation of H_2O into its ions, consistent with the kinetic model proposed by Eigen and De Maeyer.[1] A number of studies have examined water structure and dynamics confined to small pools and planar interfaces.[27,30,45-49] The current picture is that the influence of the contacting surface on the adjacent water structure is limited to about 1 nm, with water becoming bulk-like at longer distances. The hydration shell

571 and hydrogen bonding network play key roles in water ion formation and recombination
572 reactions at the molecular level.[2,9,50-53] We do not directly incorporate the molecular-level physics
573 in the kinetic description. Instead, we take advantage of the fact that the elementary rate
574 coefficients for these steps incorporate these molecular-scale influences. In particular, given that
575 recombination is diffusion-controlled,[1,3] the recombination rate coefficient contains information
576 on the detailed intermolecular interactions involved as the ions approach each other.
577 It Is known that the structure of liquids confined in pools near the interfaces that contain
578 them can be more rigid than toward the edges of the pool, leading to higher viscosity and slower
579 diffusion.[36] In the present work, however, we have no containing interfaces and therefore assume
580 that diffusion coefficients are constant throughout the volumes. Because water and water ion
581 diffusion are fast relative to local water ion generation and recombination frequencies in a small
582 volume, we model water pools as instantaneously mixed compartments of uniform composition.
583 This not only conforms to the homogeneous mixing condition that Gillespie outlined,[39,42] but
584 also simplifies analysis of the stochastics, in particular for the determination of water ion
585 populations and lifetimes as a function of water pool size. This assumption is examined in the
586 **Results Section**.
587
588 The representation of the water pools in this way carries two important characteristics.
589 First, instantaneous mixing of reactants and products in a single compartment means that water
590 ion diffusion is not represented explicitly. Second, because the particles are indistinguishable in
591 the simulation compartment, tracking the lifetimes of multiple specific ion pairs across broad
592 time and length scales requires a full 3D reaction-diffusion simulation. Kinetiscope supports such

models, however the requirement that many millions of spatial distributions be recorded to obtain useful statistics makes the simulations impractical. As an alternative, we analyze the numbers of ion pairs as a function of time to extract specific physical details. Although they are important, as noted above, we do not include interfacial interactions at this stage, focusing instead on characterizing in depth the pure water chemistry. The present model can be readily extended, however, to capture differences in ion pair formation and recombination kinetics at the interface between a water pool and another medium within a multidimensional reaction-diffusion model. Such an extension is key to applying the model to real systems, and will be made in future work as experimental and theoretical data become available to describe how interfaces affect K_w in **Eqn (2)**.

Water pool dimensions

In Kinetiscope, we model water pools using single cubic compartments. This is appropriate for water pools because we do not include interfacial physics and chemistry which would be affected by the shape of the simulation volume. The volume of a cube for a pool having a specified number of waters is calculated from the density of water at 25℃, 55.34 moles/L.[54] The range of water pool sizes used in this work is given in **Table 1**, shown for both the compartment dimension and the radius of a sphere having the same volume. This water pool size range spans that of systems where water is trapped inside reverse micelles[38] and nanopores,[55] biological cellular components,[5] porous metal organic frameworks,[56] and highly roughened electrode surfaces.[57,58]

Table 1. **Range of H_2O pools and compartment dimensions**

# of H_2O molecules	Compartment dimensions ($nm \times nm \times nm$)	Pool volume pL	Pool radius [a] R (nm)
10^3	3.11	3×10^{-11}	1.93
10^4	6.69	3×10^{-10}	4.15
10^5	14.42	3×10^{-9}	8.95
10^6	31.07	3×10^{-8}	19.28
10^7	66.95	3×10^{-7}	41.53
10^8	144.23	3×10^{-6}	89.48
10^9	310.74	3×10^{-5}	192.77
10^{10}	669.47	3×10^{-4}	415.31

[a] Calculated from the pool volume for the case where the shape is a sphere.

Water reaction kinetics

K_W as defined in **Eqn (2)** is the thermodynamic definition of the equilibrium constant. However, the equilibrium constant also has a kinetics definition, $K_{W'}$, in terms of concentrations as shown in **Eqn (9)**

$$K_{W'} = \frac{k_D}{k_R} = ¿¿¿ \tag{9}$$

where k_D is the rate coefficient for H_2O dissociation, the recombination rate coefficient k_R has been measured experimentally, and $K_{W'} = K_W / [H_2O] = 1.82 \times 10^{-16} mole/L$.[1] The true value of the water dissociation equilibrium has been a contentious topic, as has been pointed out in the literature.[59] In the thermodynamics definition, activities are used and the activity of H_2O at standard state is defined to be 1. In the chemical kinetics definition, water is treated as a reactant and its concentration (i.e. 55.34 mol/L),[54] not its activity, is used. Either value of the equilibrium coefficient is correct, so long as one consistently uses the same definition. Since we model water ion chemistry using chemical kinetics, we use $K_{W'}$. The accuracy of the rate coefficients governs

the predictive power of our model. Using an electric pulse to perturb neat water from equilibrium and measure the system relaxation time, Eigen and De Maeyer[1] measured $k_R = 1.4 \pm 0.2 \times 10^{11}$ $M^{-1}s^{-1}$ at 25℃. The measurements of k_R have proven to be robust, with multiple studies[60-62] reporting similar values within a range of 30%. k_D is too slow to be measured directly, however, so it has been calculated by multiplying $K_{W'}$ by k_R. Taking $K_{W'} = 1.82 \times 10^{-16}\, mole/L$, the rate coefficient for H_2O dissociation $k_D = 2.55 \times 10^{-5}$ s^{-1}.[1,62] We have validated our reaction model by incorporating the Eigen and De Maeyer rate constants as inputs, successfully predicting water ion concentrations of 10^{-7} mol/L (i.e. pH 7) in pools containing 10^{10} waters. Further details are provided in **SI Section S6.**

We have performed a series of calculations for 25℃ and 37℃ to examine the influence of temperature on water ion populations. The temperature dependent values for k_D were calculated using the temperature dependent values of $K_{W'}$ which are 1.82×10^{-16} at 25℃ and 4.37×10^{-16} at 37℃[5] to determine the corresponding values for k_D. The value for k_R was assumed to be constant with temperature, as indicated by experimental studies of the temperature dependence of k_R by Natzle and Moore[62] over a range from 0℃ to 48℃. At $T = 0.13 \pm 0.4$ ℃, $k_R = 6.30 \pm 0.36 \times 10^{10}$ $M^{-1}s^{-1}$, at $T = 21.1 \pm 1.2$ ℃, $k_R = 1.03 \pm 0.02 \times 10^{11}$ $M^{-1}s^{-1}$, and at $T = 47.6 \pm 0.4$ ℃, $k_R = 1.65 \times 10^{11}$ $M^{-1}s^{-1}$ (no error bars were reported at this temperature). Their data indicate that the value of $k_R = 1.4 \pm 0.2 \times 10^{11}$ $M^{-1}s^{-1}$ reported by Eigen and De Maeyer[1] at 25℃ can be used for both temperatures. Accordingly, $k_D = 2.55 \times 10^{-5}$ s^{-1} at 25℃ and 6.12 x 10^{-5} s^{-1} at 37℃.

Simulation data analysis

The calculations generate a time history for each water pool consisting of the instantaneous populations of water and water ion pairs, where the intervals between water ion formation and recombination events appear to be random. In stochastic chemical kinetics, chemical reactions follow the Markov chain model, i.e., the probability that a specific reaction step takes place is independent of the history of the system. Therefore, the simulation results for **Eqn (1)** can be analyzed as a Poisson process $P_n(t)$:

$$P_n(t)=\frac{(\lambda t)^n}{n!}e^{-\lambda t} \tag{10}$$

where t is the observation time, n is number of events that occur during the observation time, and λ is the average rate of the events taking place per unit time. Since time steps are calculated from reaction probabilities that vary continuously throughout the simulation there is variability in time intervals. In a Poisson process, the time interval between consecutive events follows an exponential decay distribution f(x; λ) where x is the time interval:

$$f(x;\lambda)=\frac{1}{\lambda}e^{\frac{-x}{\lambda}} \tag{11}$$

In the context of water ion pairs, the time interval of interest is the one between the time when water ions are formed and when they recombine. By calculating the average rate λ over a long period and extracting these intervals from the simulations and compiling their distributions, **Eqn (11)** can be used to fit the distributions to obtain a mean ion pair lifetime for a specific size of water pool.

ACKNOWLEDGMENTS

This material is based on work performed by the Liquid Sunlight Alliance, which is supported by the U.S. Department of Energy, Office of Science, Office of Basic Energy Sciences, Fuels from Sunlight Hub under Award Number DE-SC0021266. We thank Dr. Shane Ardo (UCI) for a critical reading of the manuscript.

AUTHOR CONTRIBUTIONS

FAH and WAG conceived of this study. SL and FAH performed the calculations, and all authors participated in analysis and interpretation of the simulation results. FAH and SL wrote the first draft of the manuscript and all authors participated in editing and revisions.

DECLARATIONS OF INTERESTS

The authors declare no competing interests.

INCLUSION AND DIVERSITY

We support inclusive, diverse and equitable conduct of research.

REFERENCES

1. Eigen, M., and De Maeyer, L. (1958). Self-dissociation and protonic charge transport in water and. Proc. R. Soc. Lond. A *247*, 505-533. 10.1098/rspa.1958.0208.
2. Agmon, N., Bakker, H.J., Campen, R.K., Henchman, R.H., Pohl, P., Roke, S., Thämer, M., and Hassanali, A. (2016). Protons and Hydroxide Ions in Aqueous Systems. Chem Rev *116*, 7642-7672. 10.1021/acs.chemrev.5b00736.
3. Eigen, M. (1964). Proton Transfer Acid-Base Catalysis + Enzymatic Hydrolysis .I. Elementary Processes. Angew Chem Int Edit *3*, 1-19. DOI 10.1002/anie.196400011.
4. Bronsted, J.N. (1928). Acid and Basic Catalysis. Chem Rev *5*, 231-338. 10.1021/cr60019a001.

5. Bal, W., Kurowska, E., and Maret, W. (2012). The Final Frontier of pH and the Undiscovered Country Beyond. Plos One *7*, ARTN e45832. 10.1371/journal.pone.0045832.
6. Crans, D.C., and Levinger, N.E. (2012). The Conundrum of pH in Water Nanodroplets: Sensing pH in Reverse Micelle Water Pools. Accounts Chem Res *45*, 1637-1645. 10.1021/ar200269g.
7. Silverstein, T.P. (2021). The Proton in Biochemistry: Impacts on Bioenergetics, Biophysical Chemistry, and Bioorganic Chemistry. Front. Mol. Biosci. *8*, 764099. 10.3389/fmolb.2021.764099.
8. Shon, M.J., and Cohen, A.E. (2012). Mass Action at the Single-Molecule Level. J Am Chem Soc *134*, 14618-14623. 10.1021/ja3062425.
9. Geissler, P.L., Dellago, C., Chandler, D., Hutter, J., and Parrinello, M. (2001). Autoionization in Liquid Water. Science *291*, 2121-2124. 10.1126/science.1056991.
10. Hassanali, A., Prakash, M.K., Eshet, H., and Parrinello, M. (2011). On the recombination of hydronium and hydroxide ions in water. Proc. Natl. Acad. Sci. U.S.A. *108*, 20410-20415. 10.1073/pnas.1112486108.
11. Wieder, G.M., and Marcus, R.A. (1962). Dissociation and Isomerization of Vibrationally Excited Species .2. Unimolecular Reaction Rate Theory and Its Application. J Chem Phys *37*, 1835-1852. Doi 10.1063/1.1733376.
12. Agmon, N. (1995). The Grotthuss mechanism. Chemical Physics Letters *244*, 456-462. 10.1016/0009-2614(95)00905-J.
13. Robinson, R.A., and Stokes, R.H. (1955). Electrolyte solutions; the measurement and interpretation of conductance, chemical potential and diffusion in solutions of simple electrolytes (Academic Press).
14. Urbansky, E.T., and Schock, M.R. (2000). Understanding, deriving, and computing buffer capacity. J. Chem. Educ. *77*, 1640-1644. DOI 10.1021/ed077p1640.
15. Karpe, P., and Ruckenstein, E. (1990). Effect of hydration ratio on the degree of counterion binding and pH distribution in reverse micelles with aqueous core. Journal of Colloid and Interface Science *137*, 408-424. 10.1016/0021-9797(90)90416-L.
16. Baruah, B., Roden, J.M., Sedgwick, M., Correa, N.M., Crans, D.C., and Levinger, N.E. (2006). When Is Water Not Water? Exploring Water Confined in Large Reverse Micelles Using a Highly Charged Inorganic Molecular Probe. J Am Chem Soc *128*, 12758-12765. 10.1021/ja0624319.
17. Weng, L.C., Bell, A.T., and Weber, A.Z. (2020). A systematic analysis of Cu-based membrane-electrode assemblies for CO(2)reduction through multiphysics simulation. Energ Environ Sci *13*, 3592-3606. 10.1039/d0ee01604g.
18. Monteiro, M.C.O., and Koper, M.T.M. (2021). Measuring local pH in electrochemistry. Curr Opin Electroche *25*, ARTN 100649. 10.1016/j.coelec.2020.100649.
19. Craig, R.L., Nandy, L., Axson, J.L., Dutcher, C.S., and Ault, A.P. (2017). Spectroscopic Determination of Aerosol pH from Acid-Base Equilibria in Inorganic, Organic, and Mixed Systems. J Phys Chem A *121*, 5690-5699. 10.1021/acs.jpca.7b05261.
20. Goch, W., and Bal, W. (2020). Stochastic or Not? Method To Predict and Quantify the Stochastic Effects on the Association Reaction Equilibria in Nanoscopic Systems. J. Phys. Chem. A *124*, 1421-1428. 10.1021/acs.jpca.9b09441.

21. Jin, J., Walczak, K., Singh, M.R., Karp, C., Lewis, N.S., and Xiang, C. (2014). An experimental and modeling/simulation-based evaluation of the efficiency and operational performance characteristics of an integrated, membrane-free, neutral pH solar-driven water-splitting system. Energy Environ. Sci. *7*, 3371-3380. 10.1039/C4EE01824A.
22. Nitopi, S., Bertheussen, E., Scott, S.B., Liu, X., Engstfeld, A.K., Horch, S., Seger, B., Stephens, I.E.L., Chan, K., Hahn, C., et al. (2019). Progress and Perspectives of Electrochemical CO ₂ Reduction on Copper in Aqueous Electrolyte. Chem Rev *119*, 7610-7672. 10.1021/acs.chemrev.8b00705.
23. Gupta, N., Gattrell, M., and MacDougall, B. (2006). Calculation for the cathode surface concentrations in the electrochemical reduction of CO2 in KHCO3 solutions. J Appl Electrochem *36*, 161-172. 10.1007/s10800-005-9058-y.
24. Hori, Y., Murata, A., and Takahashi, R. (1989). Formation of hydrocarbons in the electrochemical reduction of carbon dioxide at a copper electrode in aqueous solution. J. Chem. Soc., Faraday Trans. 1 *85*, 2309. 10.1039/f19898502309.
25. Yang, K.L., Kas, R., and Smith, W.A. (2019). In Situ Infrared Spectroscopy Reveals Persistent Alkalinity near Electrode Surfaces during CO2 Electroreduction. J Am Chem Soc *141*, 15891-15900. 10.1021/jacs.9b07000.
26. Wei, H.R., Vejerano, E.P., Leng, W.N., Huang, Q.S., Willner, M.R., Marr, L.C., and Vikesland, P.J. (2018). Aerosol microdroplets exhibit a stable pH gradient. P Natl Acad Sci USA *115*, 7272-7277. 10.1073/pnas.1720488115.
27. Smolentsev, N., Smit, W.J., Bakker, H.J., and Roke, S. (2017). The interfacial structure of water droplets in a hydrophobic liquid. Nat Commun *8*, ARTN 15548. 10.1038/ncomms15548.
28. Correa, N.M., Biasutti, M.A., and Silber, J.J. (1996). Micropolarity of reversed micelles: Comparison between anionic, cationic, and nonionic reversed micelles. Journal of Colloid and Interface Science *184*, 570-578. DOI 10.1006/jcis.1996.0653.
29. Luisi, P.L., Giomini, M., Pileni, M.P., and Robinson, B.H. (1988). Reverse Micelles as Hosts for Proteins and Small Molecules. Biochim Biophys Acta *947*, 209-246. Doi 10.1016/0304-4157(88)90025-1.
30. Levinger, N.E. (2002). Water in confinement. Science *298*, 1722-1723. DOI 10.1126/science.1079322.
31. Smith, R.E., and Luisi, P.L. (1980). Micellar Solubilization of Bio-Polymers in Hydrocarbon Solvents .3. Empirical Definition of an Acidity Scale in Reverse Micelles. Helv Chim Acta *63*, 2302-2311. DOI 10.1002/hlca.19800630820.
32. Mukherjee, P., Gupta, S., Rafiq, S., Yadav, R., Jain, V.K., Raval, J., and Sen, P. (2016). Ramping of pH Across the Water-Pool of a Reverse Micelle. Langmuir *32*, 1693-1699. 10.1021/acs.langmuir.5b04429.
33. Silber, J.J., Biasutti, A., Abuin, E., and Lissi, E. (1999). Interactions of small molecules with reverse micelles. Adv Colloid Interfac *82*, 189-252. Doi 10.1016/S0001-8686(99)00018-4.
34. Marques, B.S., Nucci, N.V., Dodevski, I., Wang, K.W., Athanasoula, E.A., Jorge, C., and Wand, A.J. (2014). Measurement and control of pH in the aqueous interior of reverse micelles. J Phys Chem B *118*, 2020-2031. 10.1021/jp4103349.

35. Silva, O.F., Fernández, M.A., Silber, J.J., de Rossi, R.H., and Correa, N.M. (2012). Inhibited Phenol Ionization in Reverse Micelles: Confinement Effect at the Nanometer Scale. ChemPhysChem *13*, 124-130. 10.1002/cphc.201100634.
36. Thompson, W.H. (2018). Perspective: Dynamics of confined liquids. J Chem Phys *149*, Artn 170901. 10.1063/1.5057759.
37. Maris, J.J.E., Fu, D.L., Meirer, F., and Weckhuysen, B.M. (2021). Single-molecule observation of diffusion and catalysis in nanoporous solids. Adsorption *27*, 423-452. 10.1007/s10450-020-00292-7.
38. Law, S.J., and Britton, M.M. (2012). Sizing of Reverse Micelles in Microemulsions using NMR Measurements of Diffusion. Langmuir *28*, 11699-11706. 10.1021/la300796u.
39. Gillespie, D.T. (1977). Exact stochastic simulation of coupled chemical reactions. J. Phys. Chem. *81*, 2340-2361. 10.1021/j100540a008.
40. McQuarrie, D.A. (1967). Stochastic approach to chemical kinetics. Journal of Applied Probability *4*, 413-478. 10.2307/3212214.
41. Bunker, D.L., Garrett, B., Kleindienst, T., and Long, G.S. (1974). Discrete simulation methods in combustion kinetics. Combustion and Flame *23*, 373-379. 10.1016/0010-2180(74)90120-5.
42. Gillespie, D.T. (1976). A general method for numerically simulating the stochastic time evolution of coupled chemical reactions. Journal of Computational Physics *22*, 403-434. 10.1016/0021-9991(76)90041-3.
43. Laurenzi, I.J. (2000). An analytical solution of the stochastic master equation for reversible bimolecular reaction kinetics. J Chem Phys *113*, 3315-3322. DOI 10.1063/1.1287273.
44. Hinsberg, W.D., and Houle, F.A. (2016). Kinetiscope: (http://hinsberg.net/kinetiscope/.
45. Lee, S.H., and Rossky, P.J. (1994). A comparison of the structure and dynamics of liquid water at hydrophobic and hydrophilic surfaces—a molecular dynamics simulation study. The Journal of Chemical Physics *100*, 3334-3345. 10.1063/1.466425.
46. Moilanen, D.E., Levinger, N.E., Spry, D.B., and Fayer, M.D. (2007). Confinement or the nature of the interface? Dynamics of nanoscopic water. J Am Chem Soc *129*, 14311-14318. 10.1021/ja073977d.
47. Romero-Vargas Castrillón, S., Giovambattista, N., Aksay, I.A., and Debenedetti, P.G. (2009). Evolution from Surface-Influenced to Bulk-Like Dynamics in Nanoscopically Confined Water. J. Phys. Chem. B *113*, 7973-7976. 10.1021/jp9025392.
48. Rosenfeld, D.E., and Schmuttenmaer, C.A. (2006). Dynamics of Water Confined Within Reverse Micelles. J. Phys. Chem. B *110*, 14304-14312. 10.1021/jp060552p.
49. Björneholm, O., Hansen, M.H., Hodgson, A., Liu, L.-M., Limmer, D.T., Michaelides, A., Pedevilla, P., Rossmeisl, J., Shen, H., Tocci, G., et al. (2016). Water at Interfaces. Chem Rev *116*, 7698-7726. 10.1021/acs.chemrev.6b00045.
50. Marx, D., Tuckerman, M.E., Hutter, J., and Parrinello, M. (1999). The nature of the hydrated excess proton in water. Nature *397*, 601-604. Doi 10.1038/17579.
51. Tuckerman, M.E., Marx, D., and Parrinello, M. (2002). The nature and transport mechanism of hydrated hydroxide ions in aqueous solution. Nature *417*, 925-929. DOI 10.1038/nature00797.

52. Calio, P.B., Li, C.H., and Voth, G.A. (2021). Resolving the Structural Debate for the Hydrated Excess Proton in Water. J Am Chem Soc *143*, 18672-18683. 10.1021/jacs.1c08552.
53. Hassanali, A., Giberti, F., Cuny, J., Kuhne, T.D., and Parrinello, M. (2013). Proton transfer through the water gossamer. P Natl Acad Sci USA *110*, 13723-13728. 10.1073/pnas.1306642110.
54. Wagner, W., and Pruss, A. (1993). International Equations for the Saturation Properties of Ordinary Water Substance. Revised According to the International Temperature Scale of 1990. Addendum to J. Phys. Chem. Ref. Data 16 , 893 (1987). Journal of Physical and Chemical Reference Data *22*, 783-787. 10.1063/1.555926.
55. Sun, M.H., Huang, S.Z., Chen, L.H., Li, Y., Yang, X.Y., Yuan, Z.Y., and Su, B.L. (2016). Applications of Hierarchically Structured Porous Materials from Energy Storage and Conversion, Catalysis, Photocatalysis, Adsorption, Separation, and Sensing to Biomedicine. Chem. Soc. Rev. *45*, 3479-3563. 10.1039/c6cs00135a.
56. Zhang, H.B., Nai, J.W., Yu, L., and Lou, X.W. (2017). Metal-Organic-Framework-Based Materials as Platforms for Renewable Energy and Environmental Applications. Joule *1*, 77-107. 10.1016/j.joule.2017.08.008.
57. Li, Y.G.C., Zhou, D.K., Yan, Z.F., Goncalves, R.H., Salvatore, D.A., Berlinguette, C.P., and Mallouk, T.E. (2016). Electrolysis of CO2 to Syngas in Bipolar Membrane-Based Electrochemical Cells. Acs Energy Lett *1*, 1149-1153. 10.1021/acsenergylett.6b00475.
58. Wang, L., Nitopi, S., Wong, A.B., Snider, J.L., Nielander, A.C., Morales-Guio, C.G., Orazov, M., Higgins, D.C., Hahn, C., and Jaramillo, T.F. (2019). Electrochemically converting carbon monoxide to liquid fuels by directing selectivity with electrode surface area. Nat Catal *2*, 702-708. 10.1038/s41929-019-0301-z.
59. Silverstein, T.P., and Heller, S.T. (2017). p K _a Values in the Undergraduate Curriculum: What Is the Real p K _a of Water? J. Chem. Educ. *94*, 690-695. 10.1021/acs.jchemed.6b00623.
60. Barker, G.C., Fowles, P., Sammon, D.C., and Stringer, B. (1970). Pulse radiolytic induced transient electrical conductance in liquid solutions. Part 1.—Technique and the radiolysis of water. Trans. Faraday Soc. *66*, 1498-1508. 10.1039/TF9706601498.
61. Knight, B., Goodall, D.M., and Greenhow, R.C. (1979). Single-photon vibrational photochemistry. Part 1.—Wavelength and temperature dependence of the quantum yield for the laser-induced ionization of water. J. Chem. Soc., Faraday Trans. 2 *75*, 841-856. 10.1039/F29797500841.
62. Natzle, W.C., and Moore, C.B. (1985). Recombination of hydrogen ion (H+) and hydroxide in pure liquid water. J. Phys. Chem. *89*, 2605-2612. 10.1021/j100258a035.